Optical Simulation and PSF Analysis

Yuanhao Wang

October 11, 2025

1 Experiment

For the evaluation of the results, we consider the Thorlabs LB1761 (a simple N-BK7 biconvex singlet lens) and perform a simulation using an f/8 aperture placed 2 mm from the second lens surface. We map $[R1, T, R2, D2, OD]$ (mm) as: **R1 = 24.5**, **T = 9**, **R2 = -24.5**, **D2 = 22.2**, **OD = 3.175** (f/8).

We only use **OD = 6.25 mm** for off-axis sweep and field_grid sweep.

We conducted the following experiments:

- Function test
- Layout & Ray visualization
- Best focus estimation
- Sampling number (N) sweep
- Wavelength (λ) sweep
- Through-focus (D2) sweep
- Aperture sweep (OD)
- Off-axis sweep

Further, we consider a double-Gaussian lens US2532751A, and conducted:

- Wavelength (λ) sweep
- Off-axis sweep

Function Test

Function tests are in `test_geo.py` and `test_ray_tracing.py`.

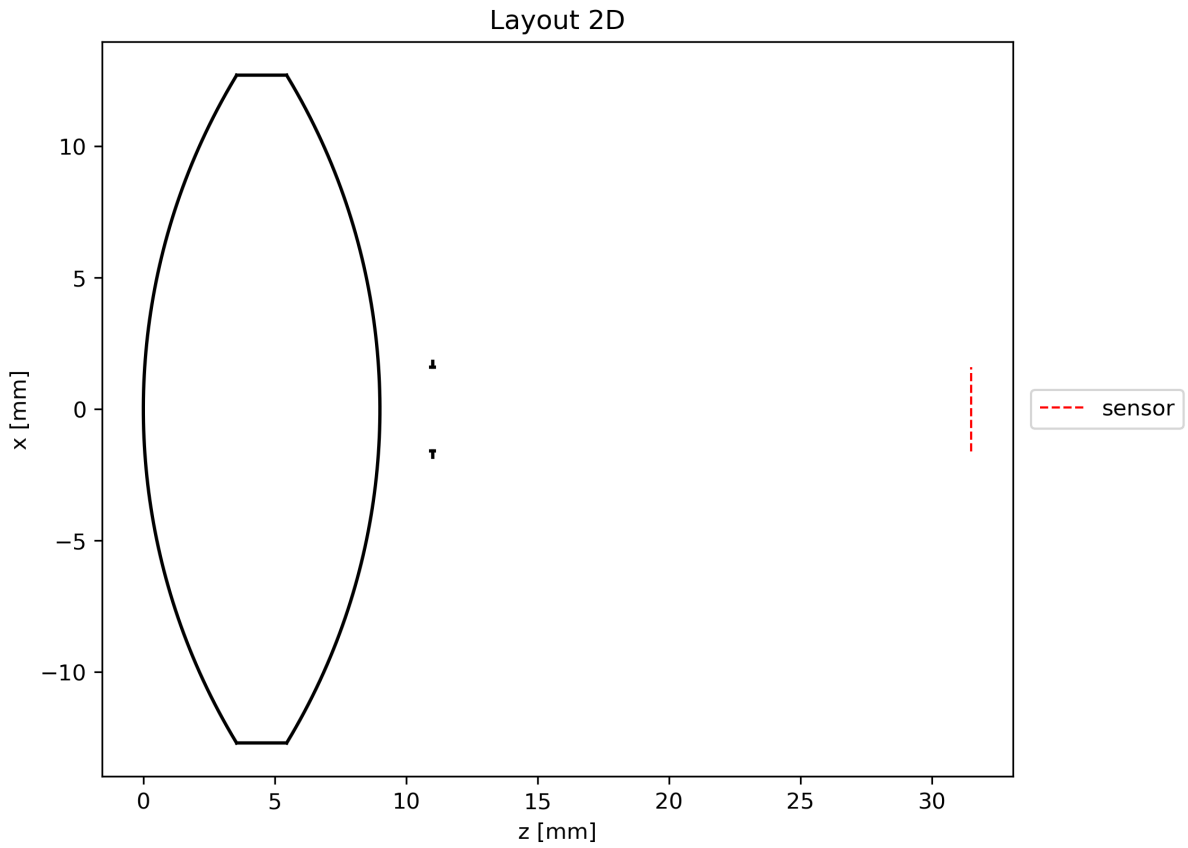

Lens layout.

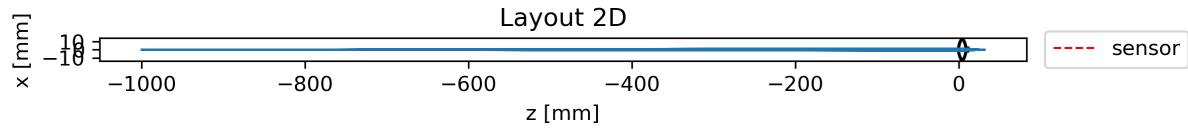

Ray tracing.

PSF Examples

After optimization, placing the sensor (mm) at the following distances *after the aperture* yields the best focus:

Table 1: Best focus distance vs. aperture

Aperture (mm)	**1.6 (f/16)**	**3.175 (f/8)**	**6.35 (f/4)**	**12.7 (f/2)**
Best Focus Distance (mm)	20.55	20.5	20.3	18.7

Observation: The best sensor-to-aperture distance varies slightly with aperture size, shifting from 20.55 mm at f/16 to 18.7 mm at f/2 due to increased spherical aberration at larger apertures.

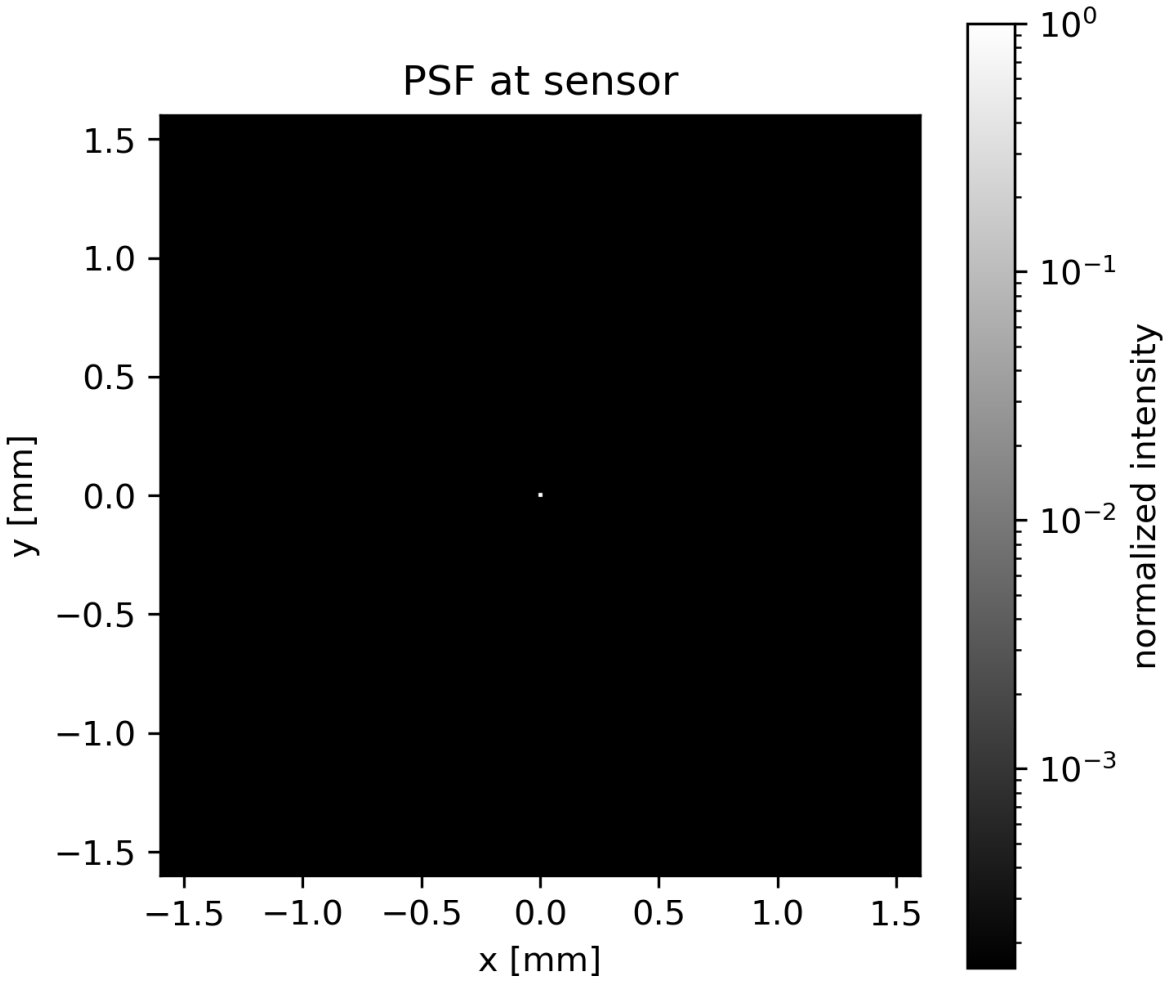

Figure 1: PSF (log scale) at best focus.

N-sweep (sampling)

We swept $N \in \{50, 100, 400, 1600, 3200, 6400\}$ and computed metrics vs. N. To probe focus sensitivity, we also used a larger aperture OD = 6.35 mm and repeated the PSF analysis.

Illustrations for $N = \{50, 400, 3200\}$ are shown below (more in the folder):

N = 50	**N = 400**	**N = 3200**
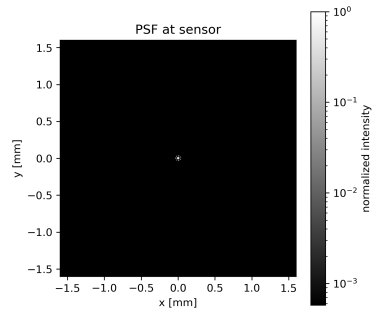	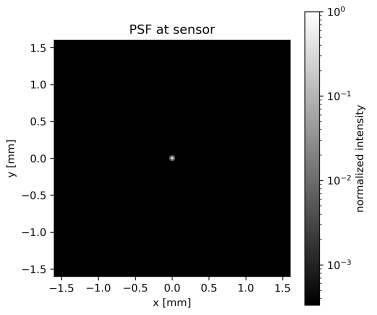	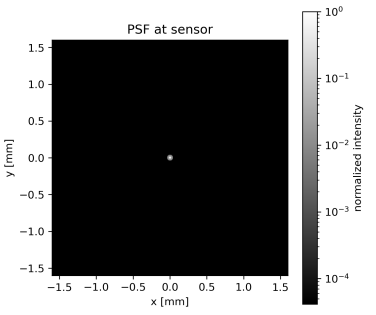

Table 2: PSF snapshots vs. sampling count N.

EE50 and RMS metrics are recorded in `metrics.csv` and plotted in:

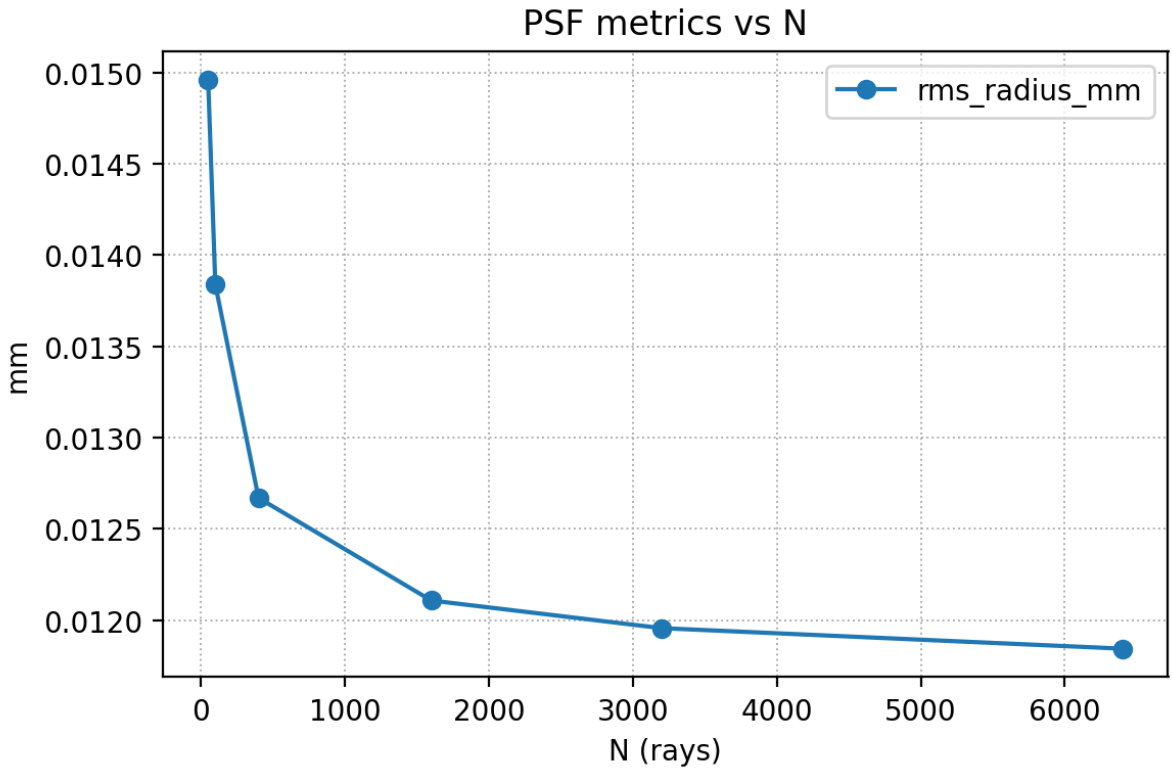

Figure 2: Metrics vs. N.

Observation: The convergence begins around $N \geq 1600$, where RMS values stabilize to $\sim 0.045\,\text{mm}$ and $\sim 0.021\,\text{mm}$, indicating sufficient ray sampling density. We choose $N = 3200$ for the remaining experiments.

Wavelength Sweep

We sweep $\lambda \in \{430, 520, 610\}\,\text{nm}$ (within the visible range):

$\lambda = 430\,\text{nm}$	$\lambda = 520\,\text{nm}$	$\lambda = 610\,\text{nm}$
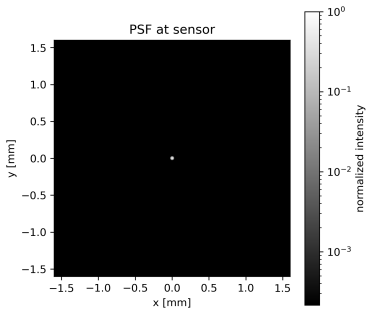	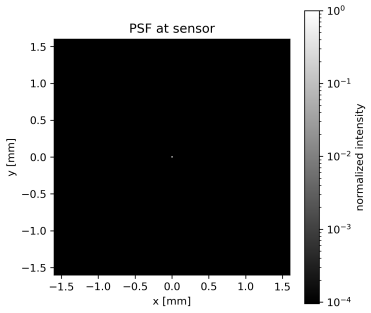	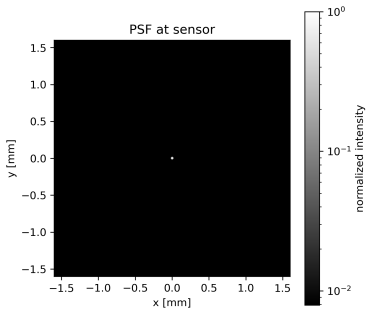

Table 3: PSF vs. wavelength.

Metrics are in `metrics.csv`; plot:

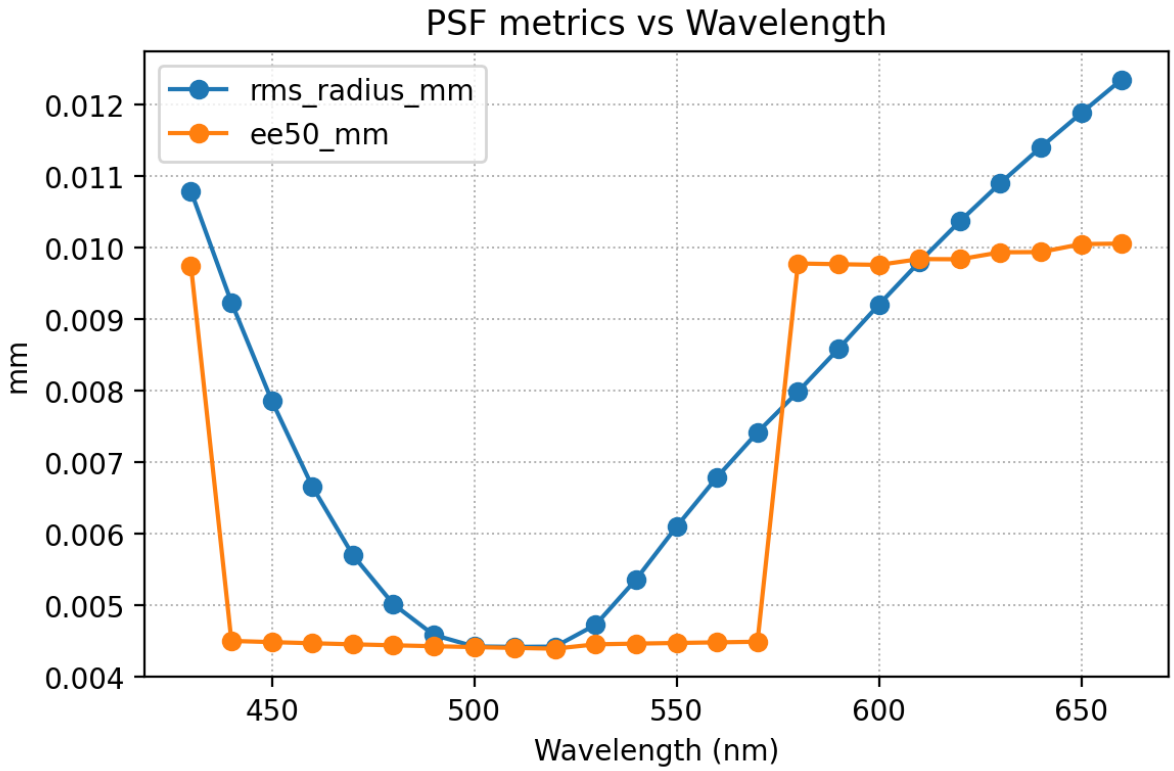

Figure 3: Metrics vs. wavelength.

Observation: With BK7 dispersion enabled, the smallest PSF occurs near $\sim 500\,\text{nm}$ and grows toward both spectral ends (chromatic focus shift).

Through-focus (D2 sweep)

We sweep $D_2 \in [19.5, 21.5]$ mm (sampling 13 steps). The best focus is at $20.5\,\text{mm}$.

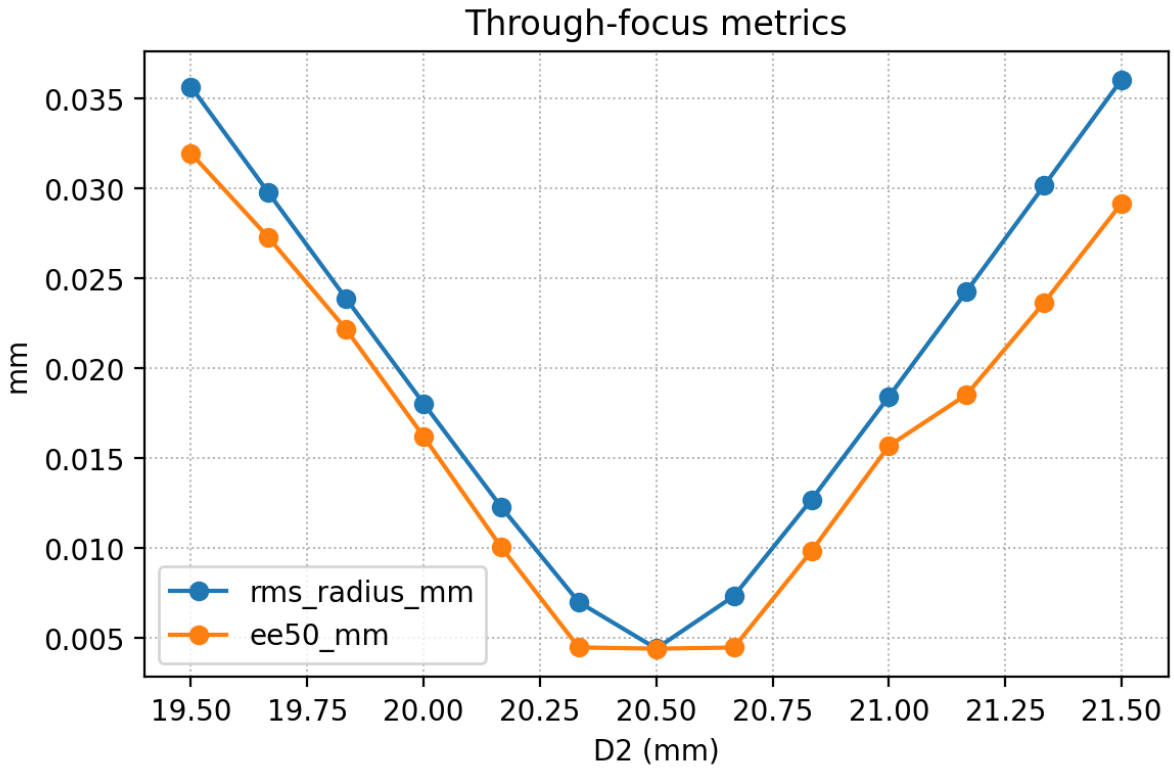

Figure 4: Metrics vs. D_2 (through-focus sweep).

Observation: Moving away from 20.5 mm (e.g., toward 20.33 or 20.66) increases RMS and EE50 smoothly; the curve is slightly asymmetric due to real lens aberrations.

Aperture Sweep (OD)

We sweep OD $\in \{1.5875$ mm $(f/16),\ 3.175$ mm $(f/8),\ 6.35$ mm $(f/4),\ 12.7$ mm $(f/2)\}$.

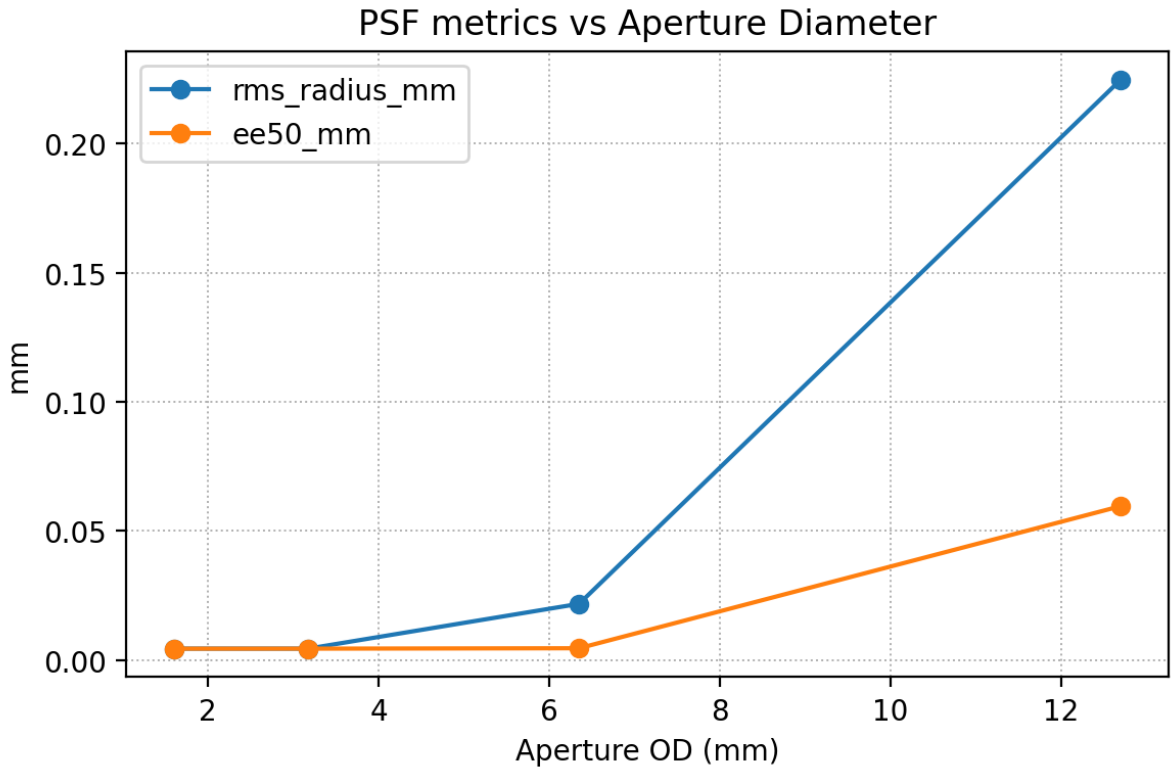

Figure 5: Metrics vs. aperture (OD).

Observation: As aperture increases from ∼1.6 to 12.7mm, the PSF core (EE50) stays nearly constant at small–moderate apertures, while the halo (RMS) grows; at the largest aperture both EE50 and RMS increase noticeably. The sharpest results occur near smaller apertures (∼1.6–3.2 mm).

Off-axis sweep

We consider OD = 6.35 mm ($f/4$) and field offsets $-35, 0, 35$ mm:

Off-axis = −35 mm	Off-axis = 0 mm	Off-axis = 35 mm
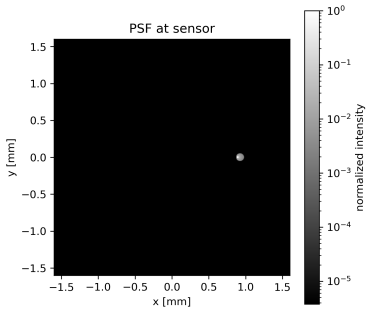	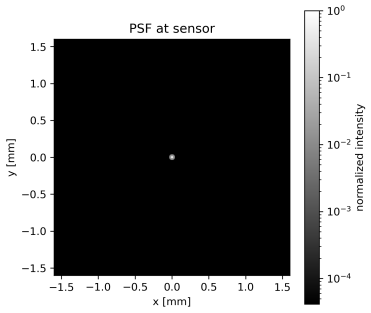	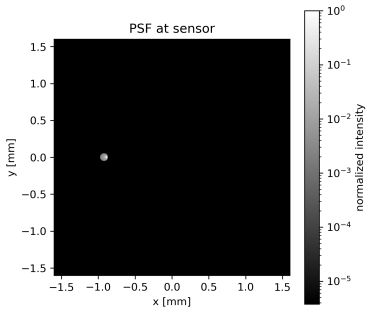

Table 4: PSF vs. field offset (biconvex).

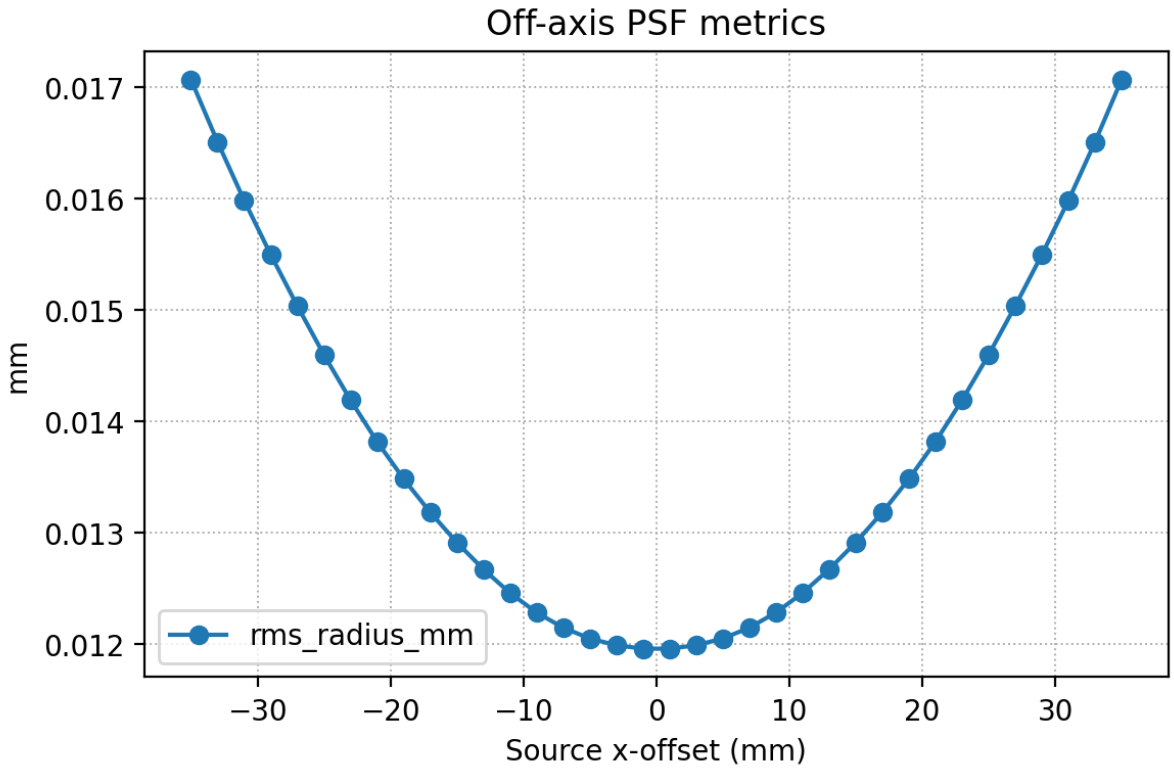

Figure 6: RMS vs. field offset.

Observation: As the source moves off-axis, the PSF centroid shifts roughly linearly with field; core size stays nearly constant for small offsets, with mild coma/asymmetry at larger field.

1.1 Discussion and Qualitative Analysis

Sampling and Aliasing

With small N, the PSF shows speckle-like noise due to non-uniform pupil mapping; as $N \gtrsim 1600$, RMS and EE50 stabilize and the PSF becomes smooth. Mitigations: increase N; average multiple seeds; sample uniformly on the pupil.

Off-Axis Source

Off-axis increases centroid shift and introduces coma/astigmatism at large field; best-focus distance varies mildly across field, indicating slight field curvature. A more complex lens group can suppress these effects.

Wavelength Dependence (Chromatic Aberration)

With BK7 dispersion, $n(\lambda)$ decreases with λ; effective focal length increases with λ. Thus a fixed sensor plane cannot be perfect for all wavelengths (blue focuses in front; red behind).

Aperture Effect (f-number)

As OD increases from f/16 to f/2: EE50 remains nearly constant at small apertures; RMS grows at large apertures due to spherical aberration and coma. This reflects a brightness–sharpness trade-off.

Through-Focus Behavior

Sweeping D_2 shows smooth degradation away from best focus (20.5 mm); curves are slightly asymmetric and steeper for larger apertures, matching expectations for residual spherical terms.

1.2 Algorithmic Correction of Aberrations

Aberrations (defocus, spherical, coma, astigmatism) broaden PSF and reduce contrast. Modeling as a spatially varying PSF $h(x, y)$, we compare classical vs. learning-based:

Table 5: Classical deconvolution vs. neural approaches

Aspect	**Classical Deconvolution**	**Neural Network Approach**
Principle	Linear inversion (e.g., Wiener, RL) with known PSF	Data-driven mapping from blurred to sharp
Pros	Interpretable; predictable; no training data	Handles complex/chromatic/field-dependent aberrations; flexible
Cons	Sensitive to noise/PSF mismatch; non-stationary PSF is hard	Needs data; potential overfitting
Best use	Mild blur, stationary PSF	Complex scenarios, data-rich pipelines

1.3 Model Refinement and Efficiency

Physical accuracy: include diffraction; model sensor pixel response (e.g., microlens/MTF); consider material tolerances (temperature).
Computation: vectorize intersections; enable GPU acceleration.
Function: extend to scene rendering.

Conclusion

The simulator reproduces key behaviors of the Thorlabs LB1761 singlet and the Double-Gauss configuration. Major outcomes:

- **Functional:** PSF metrics (RMS, EE50); even-grid alignment fix; sampling functions by object distance; `build_lens()`; modular structure; unit tests.
- **Validated optics:** Correct Snell refraction and intersections; PSF metrics converge for $N \geq 1600$; expected trends for wavelength, focus, aperture, and field.

Extra (Double-Gaussian results)

We repeat wavelength and off-axis sweeps on a Double-Gauss (aperture $\approx f/4$).

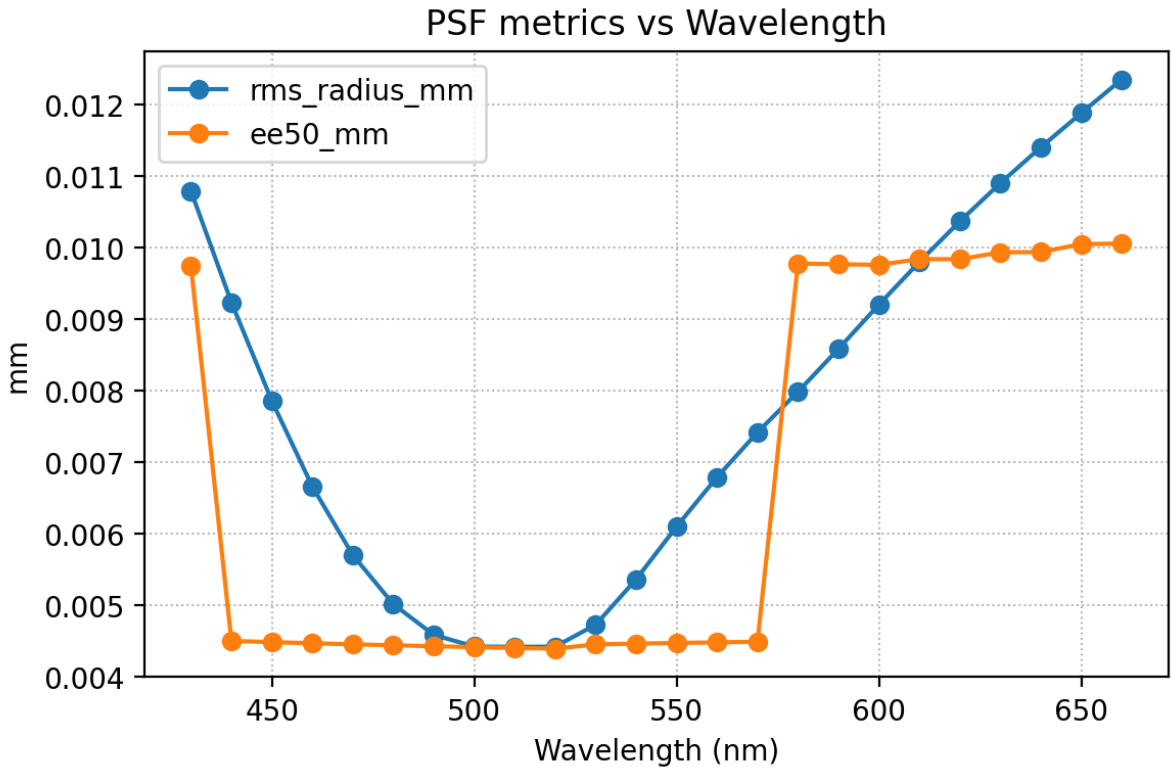

Figure 7: Double-Gauss: metrics vs. wavelength.

Wavelength sweep.

Off-axis = −35 mm	Off-axis = −1 mm	Off-axis = 35 mm
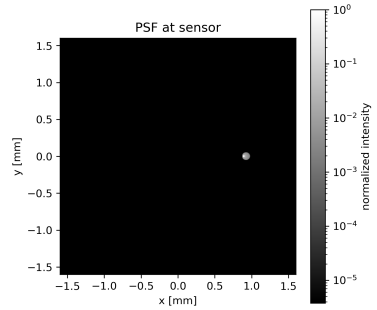	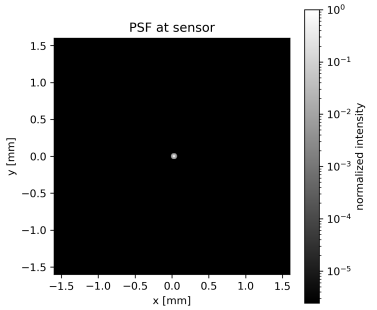	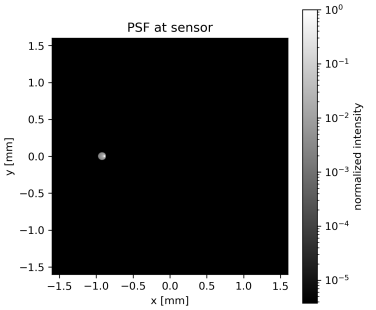

Table 6: PSF vs. field offset (Double-Gauss).

Off-axis sweep. **Observation**: With improved lens design, artifacts such as coma and other aberrations are significantly reduced, yielding better focus consistency across wavelengths—especially evident in the Double-Gauss design.